Supporting Information for:

Influence of the Ion Coordination Number on Cation Exchange Reactions with Copper Telluride Nanocrystals

Renyong Tu[1,2], Yi Xie[1,3], Giovanni Bertoni[1,4], Aidin Lak[5], Roberto Gaspari[6], Arnaldo Rapallo[7], Andrea Cavalli[6,8], Luca De Trizio*[1] and Liberato Manna*[1]

1 Department of Nanochemistry, Istituto Italiano di Tecnologia (IIT), via Morego, 30, 16163 Genova, Italy

[2] Dipartimento di Chimica e Chimica Industriale, Università degli Studi di Genova, Via Dodecaneso, 31, 16146, Genova, Italy

3 State Key Laboratory of Silicate Materials for Architectures, Wuhan University of Technology (WUT), No. 122, Luoshi Road, Wuhan 430070, P. R. China.

4 IMEM-CNR, Parco Area delle Scienze, 37/A, 43124 Parma, Italy

5 Drug Discovery and Development, Istituto Italiano di Tecnologia (IIT), via Morego, 30, 16163 Genova, Italy

6 CompuNet, Istituto Italiano di Tecnologia (IIT), via Morego, 30, 16163 Genova, Italy

7 ISMAC – Istituto per lo Studio delle Macromolecole del CNR, via Bassini 15, 20133 Milano, Italy

8 Department of Pharmacy and Biotechnology, University of Bologna, via Belmeloro 6, 40126 Bologna, Italy
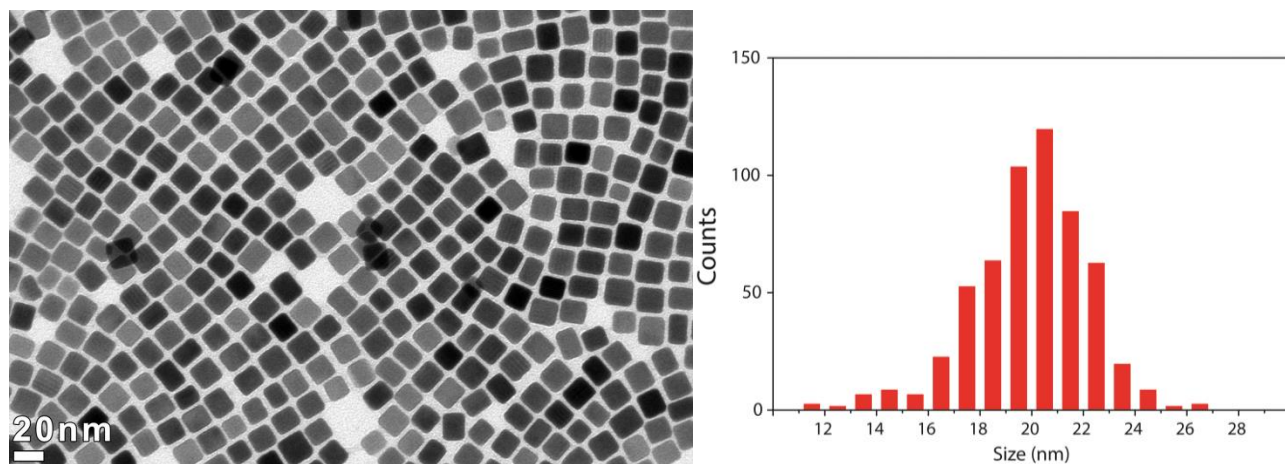
Figure S1. (left) Low resolution TEM image of as-synthesized $Cu_{2-x}Te$ NCs together with (right) their size distribution histogram.

Table S1. Summary of the CE reactions using $Cu_{2-x}Te$ NCs and Cd^{2+}, Hg^{2+}, Pb^{2+} or Sn^{2+} ions at room temperature.

$[Cd^{2+}]/[Cu^+]$ precursors ratio	TOP (mL)	NND (mL)	Reaction time (min)	Measured Composition[a]
0.2				$Cd_{0.34}Cu_{1.04}Te$
0.3	0.1	0.1	30	$Cd_{0.52}Cu_{0.80}Te$
0.4				$Cd_{0.75}Cu_{0.46}Te$
0.6				$Cd_{0.86}Cu_{0.01}Te$
$[Hg^{2+}]/[Cu^+]$ precursors ratio	TOP (mL)	NND (mL)	Reaction time (min)	Measured Composition[a]
0.15				$Hg_{0.39}Cu_{1.13}Te$
0.20				$Hg_{0.52}Cu_{0.88}Te$
0.25	0.1	0	30	$Hg_{0.63}Cu_{0.64}Te$
0.35				$Hg_{0.71}Cu_{0.41}Te$
0.5				$Hg_{0.95}Cu_{0.02}Te$
$[Pb^{2+}]/[Cu^+]$ precursors ratio	TOP (mL)	NND (mL)	Reaction time (min)	Measured Composition[a]
0.1				$Pb_{0.27}Cu_{1.23}Te$
0.2	0.1	0.1	30	$Pb_{0.45}Cu_{0.91}Te$
0.3				$Pb_{0.65}Cu_{0.55}Te$
0.5				$Pb_{1.02}Cu_{0.03}Te$
$[Sn^{2+}]/[Cu^+]$ precursors ratio	TOP (mL)	NND (mL)	Reaction time (min)	Measured Composition[a]
0.125				$Sn_{0.26}Cu_{0.89}Te$
0.25	0.1	0	30	$Sn_{0.44}Cu_{0.52}Te$
0.5				$Sn_{0.78}Cu_{0.01}Te$

[a]The composition of the NCs was calculated using ICP elemental analysis.
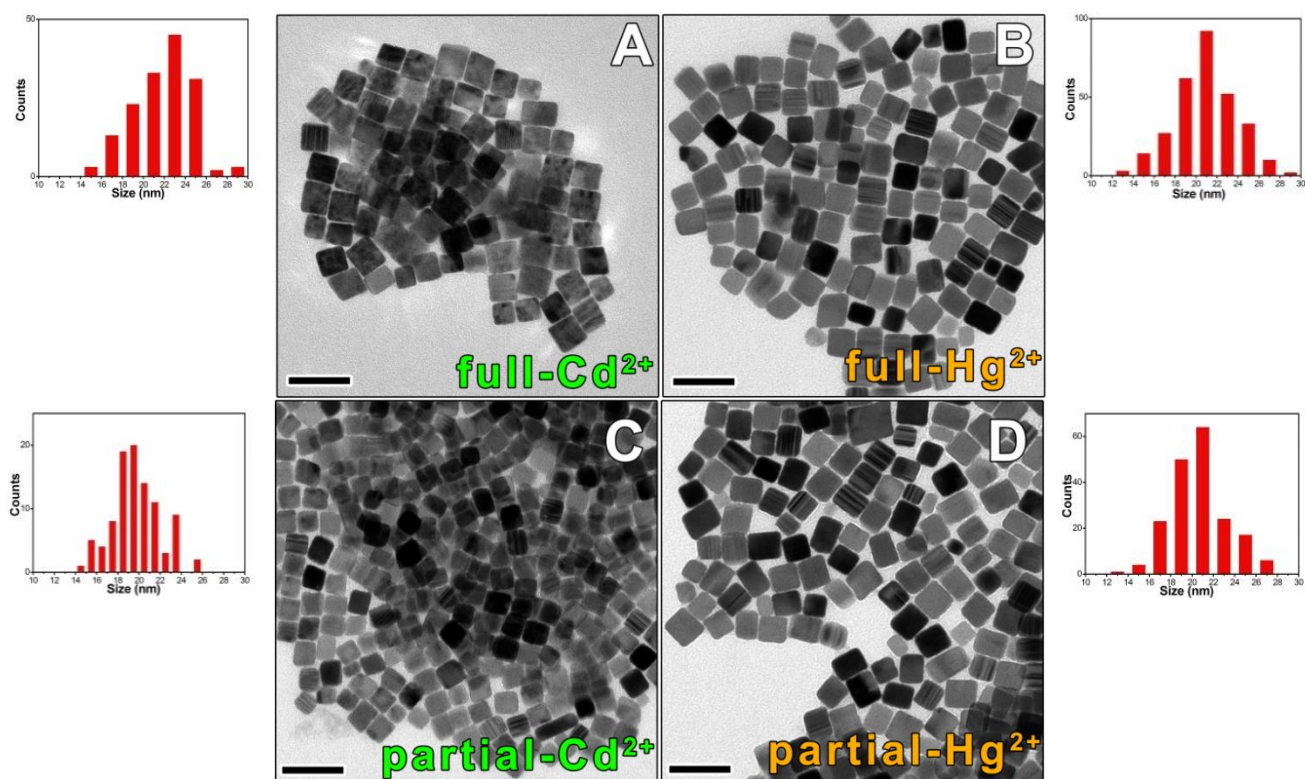
Low Resolution TEM images

Figure S2. Low resolution TEM images of CdTe (a), HgTe (b), $Cu_{2-x}Te/CdTe$ (c) and $Cu_{2-x}Te/HgTe$ (d) NCs obtained *via* CE from $Cu_{2-x}Te$ NCs and Cd^{2+} or Hg^{2+} ions. The corresponding size distribution histograms are also shown. The size distribution of NCs is: (a) 21.9±2.8 nm, (b) 20.9±2.9 nm, (c) 19.7±2.3 nm and (d) 20.7±2.6 nm. The scalebars in all the figures are 50 nm.
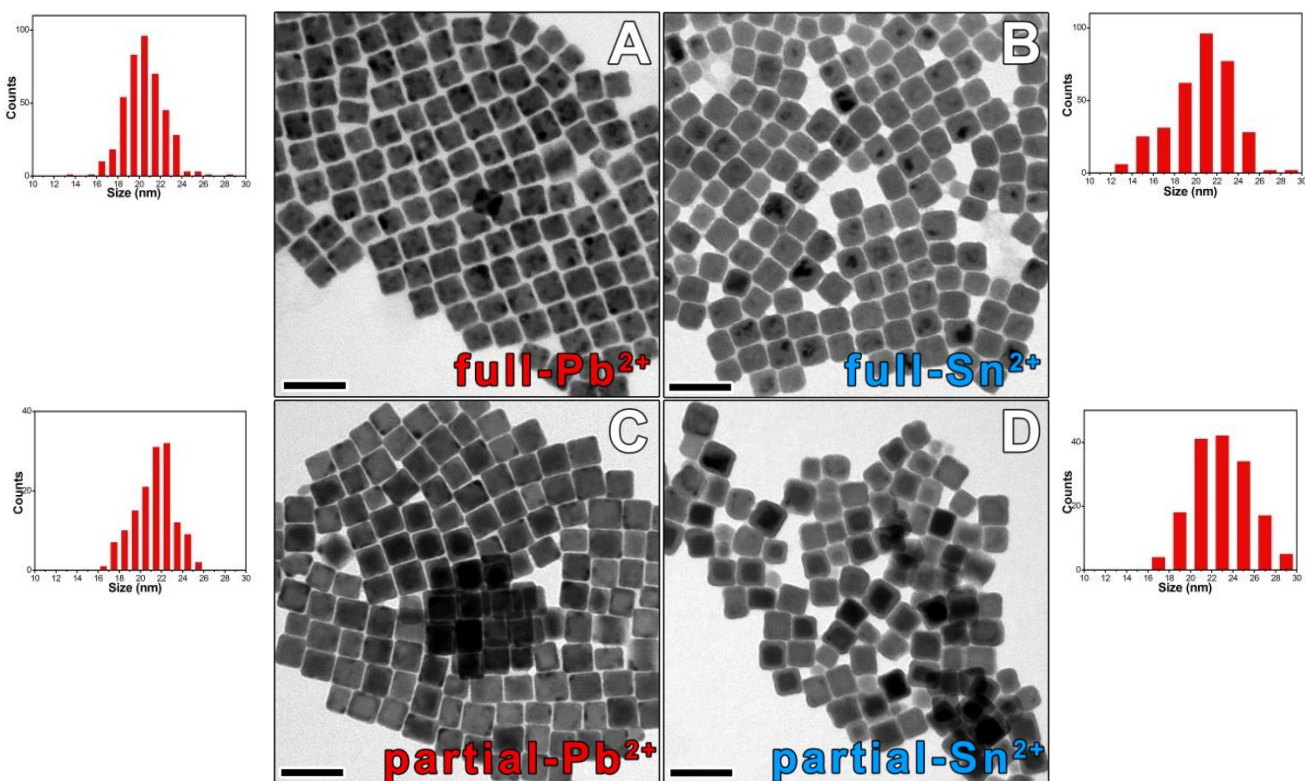

Figure S3. Low resolution TEM images of PbTe (a), SnTe (b), $Cu_{2-x}Te@PbTe$ (c) and $Cu_{2-x}Te@SnTe$ (d) NCs obtained *via* CE from $Cu_{2-x}Te$ NCs and Pb^{2+} or Sn^{2+} ions. The corresponding size distribution histograms are also shown. The size distribution of NCs is: (a) 20.5±1.8 nm, (b) 20.5±2.9 nm, (c) 21.2±2.6 nm and (d) 22.9±2.8 nm. The scalebars in all the figures are 50 nm.
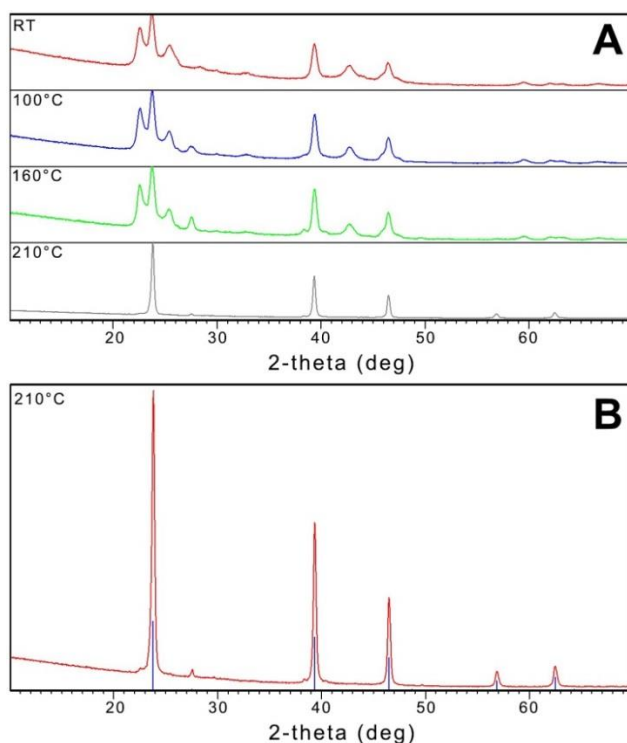
Annealing of CdTe and HgTe NCs

Figure S4. (a) XRD pattern of CdTe NCs (obtained via CE $Cu_{2-x}Te$ NCs) at RT (top pattern) and after annealing at 100 °C, 160 °C and 210°C for 30 min, respectively. (b) Zoomed XRD pattern of the sample obtained after annealing at 210°C with the corresponding bulk reflections of the cubic CdTe phase (blue bars, ICSD card 98-062-0531). The transition from hexagonal CdTe structure (at RT) to the more stable cubic one at 210°C is clearly observable.
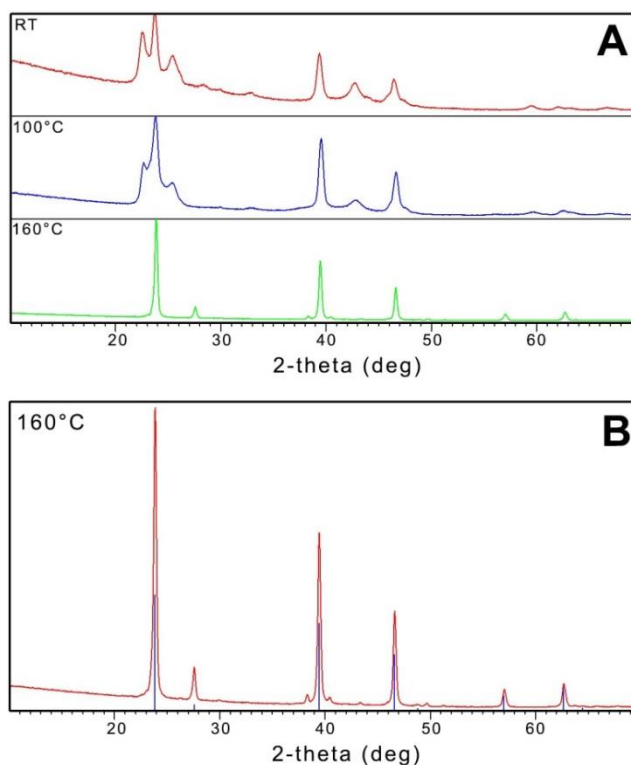

Figure S5. (a) XRD pattern of HgTe NCs (obtained via CE $Cu_{2-x}Te$ NCs) at RT (top pattern) and after annealing at 100 °C and 160 °C for 30 min, respectively. (b) Zoomed XRD pattern of the sample obtained after annealing at 160°C with the corresponding bulk reflections of the cubic HgTe phase (blue bars, ICSD card 98-016-2602). The transition from hexagonal metastable HgTe structure (at RT) to the more stable cubic one at low temperature (160°C) is clearly observable.

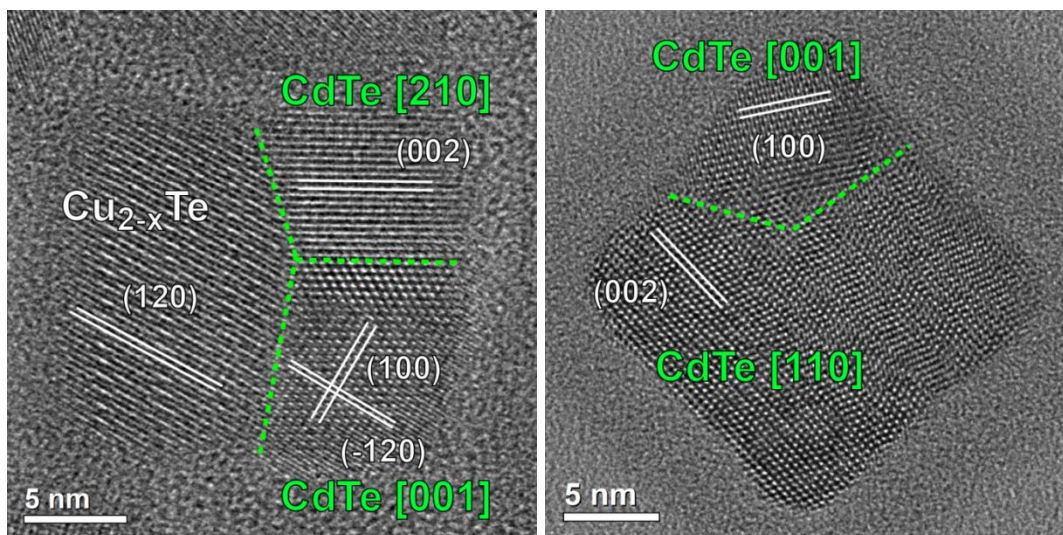**Figure S6**. (a) HRTEM image of a multi domain $Cu_{2-x}Te/CdTe$ nano heterostructure in which two main CdTe grains have formed in a single starting NC. (b) HRTEM image of a polycrystalline CdTe NC composed of two CdTe domains, most likely generated as a result of the simultaneous formation of two different CdTe nuclei at the beginning of the CE reaction of Cd^{2+} ions with $Cu_{2-x}Te$ NCs.

CE reaction between Cu₂₋ₓSe NCs and Sn²⁺ ions at RT

Synthesis of Cu$_{2-x}$Se NCs. The synthesis of Cu$_{2-x}$Se nanocrystals was carried out following our previous works with minor modifications.[1-2] In a typical reaction, 1 mmol of CuCl (0.099 g) was added to a mixture OLAM (5 mL) and ODE (5 mL) in a three neck reaction flask. The mixture was heated under vacuum for 1h at 80 °C and then heated to 300 °C under N$_2$ flow. In another reaction flask the Se precursor was freshly prepared by mixing 0.5 mmol of Se powder (0.039 g) with 5 mL of OLAM. The mixture was put under vacuum for 1 h at 150 °C and then headed to 230 °C under N$_2$ flow for 1 h to fully dissolve the Se powder. The solution, cooled down to 180 °C, was rapidly injected into the copper solution flask at 300 °C. After the injection, the reaction was kept at 300 °C for 15 min and then cooled to RT. Once at RT, 5 mL of toluene were added to the reaction mixture and the NCs were washed twice by repeated precipitation (via addition of methanol) and re-dissolution in toluene. After the last washing step, the NCs were dispersed in 3 mL of toluene and stored in a N$_2$ filled glovebox.

Partial CE experiments involving Cu$_{2-x}$Se NCs and Sn²⁺ ions. Partial CE experiments were performed following the same synthetic parameters used in the exchange reactions involving Cu$_{2-x}$Te NCs and Sn²⁺ ions. Typically, 0.1 mL of TOP was added to a 4 mL dispersion of Cu$_{2-x}$Se NCs, containing 0.02 mmol of Cu⁺, in toluene. Then 67 uL of a 0.1 M solution of Sn²⁺ in ethanol (previously prepared dissolving SnCl$_2$ in ethanol in a N$_2$ filled glove-box) were added under stirring (Sn/Cu precursors ratio is 0.3). The solution was stirred at RT for 30 min and then the NCs were washed twice via precipitation with addition of ethanol followed by re-dissolution in toluene (note: in each washing step, 0.05 mL OLAM was added to stabilize the NCs). The composition of the resulting NCs, measured by ICP elemental analysis, resulted to be Sn$_{0.49}$Cu$_{0.75}$Se (that is SnSe/Cu$_{1.53}$Se).
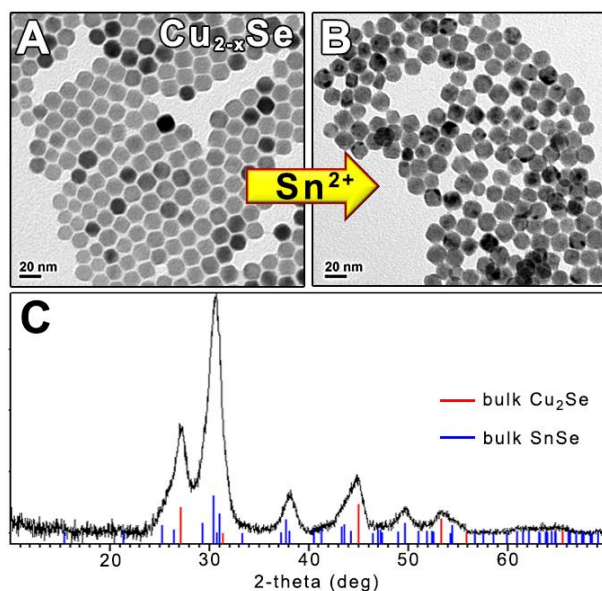

Figure S7. Low resolution TEM images of Cu$_{2-x}$Se NCs before (a) and after (b) partial CE with Sn²⁺ ions at RT. (c) X-ray diffraction pattern obtained from dropcast solution of Sn²⁺-partially exchanged Cu$_{2-x}$Se NCs with the corresponding bulk reflections of berzelianite Cu$_2$Se (red, ICSD number 98-004-1140) and orthorhombic SnSe (blue, ICSD number 98-005-0542).
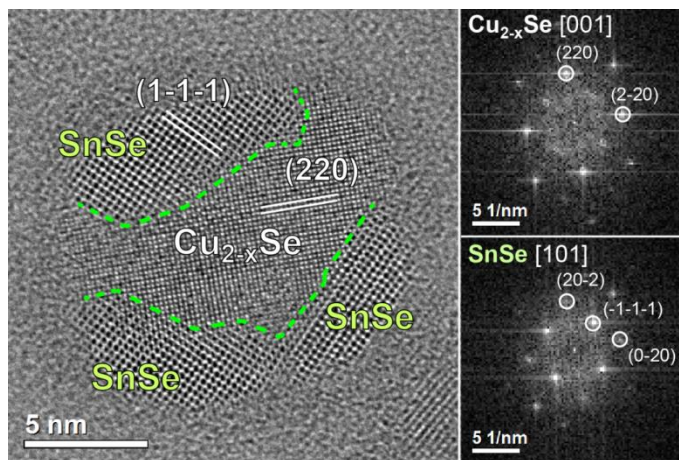

Figure S8. High resolution TEM image of a Cu$_{2-x}$Se-SnSe NHC obtained via partial CE of Cu$_{2-x}$Se NCs with Sn²⁺ cations. The nucleation of the product SnSe phase occurs unselectively on the surface of the starting Cu$_{2-x}$Se NC. The green dashed line indi-

cates the border between the central $Cu_{2-x}Se$ and the surrounding SnSe domains. On the right side the two FFTs are shown, demonstrating the good epitaxial relationship between the structures.
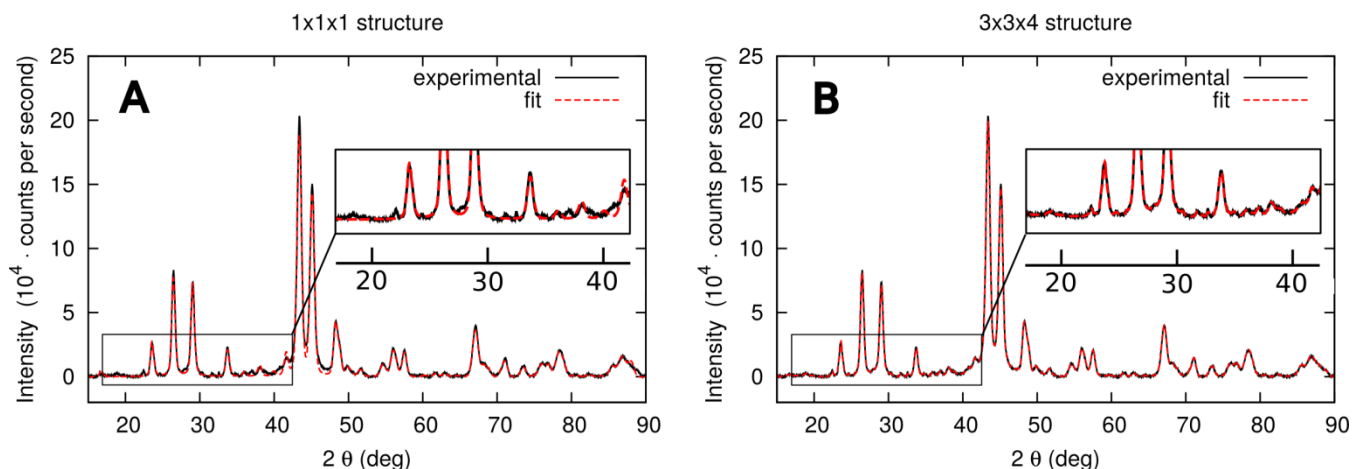
XRD pattern indexing

Figure S9. Le Bail fit of the (a) 1×1×1 basic cubic structure and (b) of the 3×3×4 superstructure XRD pattern.[3] 20 Le Bail cycles have been performed and all parameters of the fit have been optimized by the software Fox.[4] The disagreement factor calculated considering the 1×1×1 basic cubic structure is 0.08973, while in case of the 3×3×4 superstructure is 0.01931

Pindex is a house-made program implementing an indexing procedure based on Monte Carlo sampling. It is an iterative method inspired by the multicanonical approach which samples the space of the cell parameters and accumulates the histograms of a disagreement factor during the iterations.[5] The disagreement factor is defined as a function in (0,1) of the absolute deviations between calculated and experimental peaks positions. The cells are ranked according to the ascending order of the disagreement factor, lower values meaning better cells. Also, it is possible to rank the cells on the basis of the difference between calculated and certain reference cell geometrical features assumed as known in advance.[6] The histograms collected during the various iterations are used as biases for the sampling, such that the cells proposed by the Monte Carlo moves become better and better as the iterations proceed. Trials on different cases showed that the cell searches greatly benefit from the application of biases to the Monte Carlo random walks, especially in low symmetry cases.

Table S2. Indexing of the cubic structure. Θ_{exp} is the experimental diffraction angle at which a peak is observed. Most experimental peaks can be matched at an angle (θ_{cal}) at which a specific (h,k,l) reflection of the model cell occurs. Some experimental peaks cannot be indexed by the use of a small cubic cell, this being due to the superstructure highlighted by the HRTEM analysis. z_{sft} is the zero shift of the diffraction angle.

h	k	l	$2\theta_{exp}$	$2\theta_{cal}$	$2\theta_{cal}+z_{sft}$	$2\theta_{exp}-2\theta_{cal}-z_{sft}$
0	0	-1	16.740	16.721	16.704	0.0363
			18.793			
			22.450			
0	-2	0	23.601	23.613	23.595	0.0054
			24.596			
0	-2	-1	26.467	26.481	26.464	0.0027
			27.963			
-1	-2	-1	29.046	29.074	29.057	0.0107
			30.338			
			31.625			
			32.548			
0	-2	-2	33.723	33.747	33.730	0.0069
			34.817			
0	0	-3	35.996	35.976	35.959	0.0362
			37.015			
-1	0	-3	38.081	37.985	37.968	0.1133
			38.850			
			40.810			
-2	-2	-2	41.657	41.656	41.639	0.0182
-3	-2	0	43.390	43.408	43.391	0.0008
-3	-2	-1	45.130	45.147	45.130	0.0005
0	-4	0	48.294	48.310	48.293	0.0012
-1	-4	0	49.852	49.908	49.891	0.0388
-4	-1	-1	51.661	51.650	51.633	0.0282
-4	-2	0	54.640	54.629	54.612	0.0279
-4	-2	-1	56.032	56.105	56.088	0.0560
-2	-3	-3	57.531	57.553	57.536	0.0045
			59.676			
-4	-3	0	61.691	61.692	61.675	0.0159
0	-5	-1	62.885	62.901	62.884	0.0007
-5	-1	-1	64.564	64.490	64.473	0.0915
-5	-2	0	67.099	67.103	67.086	0.0133
-2	-5	-1	68.144	68.212	68.195	0.0508
-4	0	-4	71.111	71.126	71.108	0.0021
-4	-3	-3	73.536	73.533	73.516	0.0205
-6	0	0	76.040	76.064	76.047	0.0070
-1	-6	0	76.835	76.974	76.957	0.1220
-5	-3	-2	78.454	78.484	78.467	0.0131
-2	-6	0	80.611	80.670	80.653	0.0415
-5	0	-4	82.343	82.316	82.299	0.0440
2	-6	-2	85.608	85.564	85.547	0.0615
-2	-5	-4	86.914	86.946	86.929	0.0151

REFERENCES

(1) Deka, S.; Miszta, K.; Dorfs, D.; Genovese, A.; Bertoni, G.; Manna, L. *Nano Lett.* **2010**, *10*, 3770-3776.

(2) Dorfs, D.; Härtling, T.; Miszta, K.; Bigall, N. C.; Kim, M. R.; Genovese, A.; Falqui, A.; Povia, M.; Manna, L. *J. Am. Chem. Soc.* **2011**, *133*, 11175-11180.

(3) Le Bail, A. *J. Solid State Chem.* **1989**, *83*, 267-271.

(4) Favre-Nicolin, V.; Cerny, R. *J. Appl. Crystallogr.* **2002**, *35*, 734-743.

(5) Berg, B. A.; Neuhaus, T. *Phys. Lett. B* **1991**, *267*, 249-253.

(6) Rapallo, A.; Ricci, G.; Porzio, W.; Arrighetti, G.; Leone, G. *Cryst. Growth Des.* **2014**, *14*, 5767-5772.